Published in Soil Dynamics and Earthquake Engineering

Post-Print version of:

Reuland, Y., Lestuzzi, P., Smith, I.F.C., 2019. A model-based data-interpretation framework for post-earthquake building assessment with scarce measurement data. Soil Dynamics and Earthquake Engineering 116, 253 -263. https://doi.org/10.1016/j.soildyn.2018.10.008

A model-based data-interpretation framework for post-earthquake building assessment with scarce measurement data

Yves Reuland[a,*], Pierino Lestuzzi[a], Ian F.C. Smith[a]

[a] *Applied Computing and Mechanics Laboratory (IMAC), School of Architecture, Civil and Environmental Engineering (ENAC), Swiss Federal Institute of Technology (EPFL), Lausanne, Switzerland*

Abstract

Recent earthquake events throughout the world have once again exposed the vulnerability of buildings with respect to earthquakes. It is unlikely and unsustainable to design and - especially in regions with low-to-moderate seismic hazard - to retrofit all buildings to remain within elastic displacement ranges during earthquakes with high return periods. Therefore, post-earthquake assessment plays a fundamental role in the resilience of cities, given the potential to reduce time between an earthquake event and the clearance for (renewed) occupancy of a building. In this paper, a framework for model-based data interpretation of measurements of earthquake-damaged structures is presented. The framework allows engineers to combine ambient-vibration measurements and visual inspection to reduce parametric uncertainty of a high-fidelity model using the error-domain model-falsification methodology. For building types that have limited stiffness contributions from non-structural elements (i.e. shear-wall buildings) and for which non-ductile failure modes (such as out-of-plane failure) can be excluded, reduction in natural frequency and damage grades derived from visual inspection provide global measurement sources for structural identification. The application of the proposed methodology to a shear-resisting building tested on a shake table illustrates that vulnerability-curve predictions provide accurate damage estimates for subsequent earthquakes with probabilities between 50 and 100 percent for five measured scenarios. In complete absence of baseline information regarding the initial building state and the earthquake signal, parametric uncertainty is reduced by up to 76 percent. This study thus demonstrates usefulness for certain building types to enhance post-seismic vulnerability predictions.

Keywords: Model-based data interpretation, Post-earthquake building assessment, Scarce measurement data, Seismic vulnerability of existing buildings, Static nonlinear analysis, Parametric uncertainties, Ambient-vibration measurements

*Corresponding author

Email address: yves.reuland@epfl.ch (Yves Reuland)

1. Introduction

Recent earthquake events across the world have exposed the continuing earthquake-related threats to built infrastructure. Despite improvements to building codes, existing buildings have often been built either with inadequate assumptions regarding earthquake actions or without any seismic consideration (especially in regions with low-to-moderate seismic hazard). Therefore, earthquake events are likely be followed by significant post-seismic assessment activities. Current practice for such assessment relies on visual inspection, which has several shortcomings. In addition to being potentially subjective [1, 2], visual inspection is slow [3] and usually provides information that is limited to how a building behaved during the earthquake rather than contributing to quantitative estimates of vulnerability with respect to future seismic actions [4]. Little effort has focused on evaluating the residual capacities of damaged structures to withstand future earthquake actions. However, the imminent risk of aftershocks (as shown by the recent earthquake sequence in Italy [5] with nine events exceeding magnitude 5.0 from August 2016 to April 2017) and the gradual deterioration of structures due to earthquake sequences justifies residual-capacity assessments with respect to future actions.

Visual inspection alone may be insufficient for accurate and objective assessment of the residual seismic capacity of buildings. Building owners often ask for detailed engineering evaluations regardless of the outcome of visual screening [6]. Model-based measurement interpretation has the potential to reduce the uncertainty related to structural behavior. Such uncertainties can undermine the accuracy and precision of detailed engineering evaluations. However, despite growing popularity of smart-city applications and increased availabilty of affordable sensors, it is unlikely that large parts of the building stock will be equipped with permanent measurement systems soon. Such permanently installed sensors would provide the engineers with measurement data before, during and in the immediate aftermath of an earthquake. In absence of such detailed data, ambient-vibration measurements are recommended as an objective data source to complement visual inspections. Indeed, differences in fundamental frequencies have been found to be indicators of structural damage in the past [7, 8, 9, 10]. Dunand et al. [11] were the first to propose ambient vibrations as a complement for visual inspection to classify buildings in the aftermath of an earthquake. Model-based measurement-interpretation techniques can help combine engineering knowledge (model) with observed behavior (measurements). This paper contains a description of a methodology that exclusively employs post-earthquake evidence (visual inspection and ambient-vibration measurements) to reduce the uncertainty on the residual seismic capacity of earthquake-hit structures. However, as structures must experience a reduction in stiffness prior to failure, the scope of the methodology is currently limited to shear-resisting buildings that have low stiffness contributions from non-structural elements.

In the past, much research effort has focussed on measurement-based damage detection and damage identification of earthquake-hit structures [12, 13, 14, 15, 16]. Model-based localisation and quantification of damage using vibration measurements is usually performed by updating parameter values of a linear finite element model [17, 18, 19]. However, such an approach implies that a large number of individual damage parameters are known [15]. Methods for damage detection based on modal properties were also proposed for cases without baseline (intact) measurement data [20, 21]. Nozari et al. [22] proposed a non-deterministic approach in damage identification due to variability

in ambient-vibration data. However, by relying on linear elastic models, such damage identification approaches fail to provide accurate and useful predictions of the behavior of a structure under future earthquakes. In addition, they claim that since initial and damaged states are compared, model uncertainties that arise from omissions and simplifications, such as influence of boundary conditions and non-structural elements, can be neglected [23]. Few contributions stated that modelling uncertainty undermines vibration-based damage detection [24, 25, 26]. Behmanesh and Moaveni [27] found that increasing levels of damage lead to a decrease in the identification efficiency and accuracy. However, in absence of initial measurements and in predicting the behavior under future earthquakes (extrapolation), model uncertainties need to be carefully evaluated and transparently integrated into model-measurement comparison strategies. Damage detection or anomaly detection was also performed using model-free techniques [28, 29, 30, 31] that fail ensure behavior extrapolation, such as prediction of the structural response under future earthquake actions and designing repair activities as well as retrofitting for deteriorated buildings.

Recently, the evaluation of the vulnerability increase of earthquake-damaged structures with regard to aftershocks received attention, mostly for performance-based design [32]. In addition, updated vulnerability assessments for buildings characterized by a given damage state after a main-shock have been proposed [33, 34, 35]. Trevlopoulos and Guéguen [36] proposed an operational forecasting of vulnerability through a sequence of aftershocks based on measured period elongation. However, few studies incorporate measurement interpretation to update vulnerability curves after the main shock. In addition, uncertainties are generally limited to ground-motion parameters, and do not include behavior-modelling uncertainties.

In this paper, error-domain model falsification (EDMF) is used for data interpretation (comparison of model simulations with measured behavior). Observations from two sources of different nature, subjective and approximate visual inspection as well as objective and precise post-earthquake modal quantities are combined in order to reduce the uncertainty regarding residual seismic capacity. Goulet et al. [37] formalized the idea of using data to falsify wrong models instead of optimizing single models, which lead to the development of a data interpretation technique, called EDMF, that accommodates modelling and measurement errors that contain systematic bias [38]. EDMF has been shown in the past to provide accurate prediction results in case of extrapolation in presence of large uncertainties [39, 40].

This paper starts with a description of an iterative and sequence-free data-interpretation framework for post-earthquake assessment (Section 2). Most important elements of the framework are presented: EDMF (Section 2.1), nonlinear models based on AEM (Section 2.2), use of static nonlinear prediction for vulnerability assessment (Section 2.3), combination of visual inspection and modal properties (Section 2.4), and iterative introduction of measured information (Section 2.5). The proposed framework is tested on a half-scale laboratory specimen (Section 3).

2. An iterative and sequence-free framework for post-earthquake assessment of structures using static nonlinear predictions

A framework for model-based data interpretation in a post-earthquake context is presented in this section. An existing framework for linear measurements and predictions of bridge behavior [41] is built upon, adapted and extended. The methodology proposed

in this paper relies on static nonlinear predictions and measurement data that can be gathered in the aftermath of an earthquake and thus, is limited to visual inspection and post-earthquake natural frequencies. The aim of implementing a data-interpretation technique is to reduce the parametric uncertainty of a physics-based model. Data interpretation that is based on nonlinear behavior models involves engineering judgement at multiple stages. Thus, the engineer is placed at the centre of the iterative framework that is proposed in Figure 1. The main components of data interpretation, which are iteratively revisited by the engineer, are: a physics-based model; structural measurements; in-situ inspections; a data-interpretation methodology (EDMF); and behavior prognosis under future loading events. Finally, upon the vulnerability predictions that are made using the physics-based model, stakeholders and governing bodies take decisions regarding safety for occupancy of buildings.

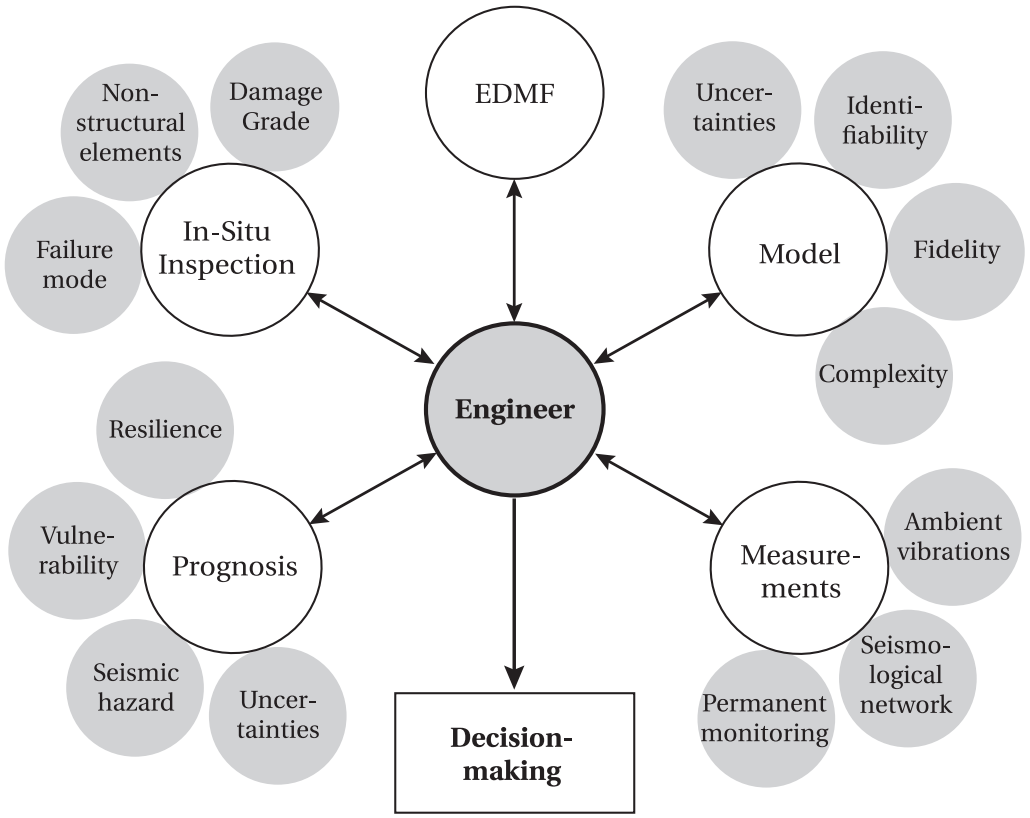

Figure 1: Iterative and sequence-free framework for asset management of earthquake-damaged structures. The engineer is at the center and evaluates and re-evaluates data sources, uncertainties, model classes, visual information, model predictions using EDMF in order to reach robust and objective decisions.

As stated before, a physics-based model (see Section 2.2) is used to extrapolate structural behavior under future earthquake actions. Within the scope of this paper, the measurements and in-situ inspections are limited to the post-seismic building state.

The proposed framework relies on iteratively revisiting several stages that form part of data-interpretation applications. Model predictions and measured evidence are compared using EDMF and, depending on the outcome of model falsification (see Section 2.1) the engineer decides upon the following steps. Structural identification and behavior predictions are performed using static nonlinear model predictions. In this paper, a high-fidelity nonlinear model is used for model predictions. While the framework can be applied to a large range of nonlinear model classes (defined by inherent model fidelity), selection of a specific model class and the related consequences on model predictions are not within the scope of this paper.

The utility of in-situ inspection to assess the state of a building is manifold: replacing in-situ visual observations with an automated and remote analysis of structural measurements is not proposed. For example, danger from falling debris that often come from secondary elements cannot be assessed by structural models of a building, since non-structural elements are generally excluded from simulation models. Rapid visual screening is an assessment tool that provides useful post-earthquake evaluation of buildings for immediate occupancy and crisis management. Although it has limitations regarding residual capacity of deteriorated buildings (as discussed in the introduction, Section 1), the outcomes of visual inspection are tightly integrated into the framework. In addition, numerical models often implicitly involve assumptions related to structural behavior, especially with regard to failure modes. Expert-conducted visual inspection either bolsters such assumptions or indicates presence of more likely failure modes. Also, predicted locations of damage can be compared to the observed damage in order to validate models. As some failure modes (such as loss of bond between concrete and reinforcement bars) do not have a significant influence on building stiffness, their detection through vibration measurements is not dependable. Alternative assessment tools are needed to help engineers in detecting the presence of such failure modes.

In the past, outcomes of visual inspection have been linked to physical quantities of buildings. For example, the European Macroseismic Scale (EMS98) defines five damage grades (DG) that can be observed through visual inspection [42] and that have been linked to mechanical parameters of the structure [43]. Therefore, DGs can be considered a data source for structural identification. As higher DGs involve ultimate displacement or rotation, they add valuable information regarding nonlinear ultimate states of the structure. Also, DGs provide a link between the initial and post-earthquake buildings states and thus, alleviate the need for initial modal properties that are often not available.

In a similar way to modal properties, DGs provide a global score to the damage a building sustained during an earthquake (the general DG is a weighted average over the whole building). Therefore, local failure mechanisms have little effect on the reported DG. In addition, a calculated approximate DG will not replace in-situ inspection, since local mechanisms and falling debris that are potential sources of danger are not recognised. Especially in unreinforced masonry buildings, local mechanisms may lead to important damage and potentially, to collapse.

2.1. Error-domain model falsification

Relying on EDMF as the basis of the proposed framework for residual-capacity estimation results from several strengths of the EDMF methodology:

- EDMF provides robustness with respect to unknown correlations between model uncertainties of various sources [39].
- The expected utility of an additional data source can help the engineer to choose between several data sources, such as material testing, ambient vibration measurements or refined site analysis for soil-structure interactions.
- Upon availability, EDMF allows the engineer to incorporate additional information, such as the outcome of a detailed in-situ inspection, easily and explicitly. Availability of new measurements or re-evaluating uncertainty distributions does not require additional simulation runs.
- Engineers are able to combine various types of measurement data with different forms and levels of uncertainty. When conservative bounds on uncertainty are estimated, EDMF offers accurate identification results, as has been shown in the past [39, 40].
- Observed DGs typically result in ranges of possible maximum displacements during an earthquake. Within such ranges all displacement values are equally likely and thus, informed likelihood functions (such as Gaussian distributions) that form part of other structural-identification methodologies are not compatible with this context.
- Unlike other engineering structures, such as high-rise buildings and bridges, ambient-vibration measurements on low to medium rise buildings usually result in characterising less than five vibration modes. Generally, data-interpretation techniques require more measurement data points to provide accurate results. With conservative uncertainty estimations, use of EDMF involves lower precision than other population approaches in order to provide accuracy and robustness in contexts where there is a low number of measurements.
- An EDMF-based framework is compatible with engineering practice that typically involves reasoning with models at various levels of approximation.

2.1.1. Background of error-domain model falsification

The model falsification approach has been built upon the strategy that measurement data should ideally be used to discard (or falsify) inappropriate models instead of validating models - a concept in accordance with the principles of scientific discovery [44]. Thus, a multi-model strategy has been introduced into data interpretation [45, 46]. As not every every relevant phenomenon and physical parameter that influences the behavior of complex full-scale structures can be included in structural models, falsification thresholds are calculated to discard model instances.

Simplifications and omissions result in a model error value, u_g, which characterises the model class $g(.)$. Similarly, measurement data $\hat{y}$ is subject to a measurement error u_y. Given the parameter values, θ^*, for the model $g(.)$ are known, and the model error value u_g is known, the true structural response equals the sum of the model prediction, $g_i(\theta^*)$, and the model error, $u_{g,i}$. In a similar way, the true structural response equals the sum of the measured value, $\hat{y}_i$, and the measurement error, $u_{y,i}$, thus leading to Equation 1 for every measured quantity i.

$$g_i(\theta^*) + u_{g,i} = \hat{y}_i + u_{y,i}, \forall i = 1, 2, ..., n_m \quad (1)$$

The complexity of full-scale engineering structures and their response to unmodelled conditions hinders precise knowledge of the model and measurement error values. Due to the absence of precise information related to error values, they are characterised by random variables: U_g for model uncertainty and $U_{\hat{y}}$ for measurement uncertainty. A joint probability density function, $f_{U_c}(U_c) \sim U_{\hat{y}} - U_g$, is obtained by combining measurement and modelling uncertainty. The joint PDF, f_{U_c}, is generally dominated by model uncertainties, which have much higher variances than measurement uncertainties [47]. Also, unlike measurement uncertainties, model uncertainties are often biased (non-zero mean distributions).

Based on the joint distribution, $f_{U_c}(U_c)$, lower and upper thresholds, $T_{low,i}$ and $T_{high,i}$, are derived and delimitate the shortest interval corresponding to a target probability ϕ_d (see Eq. 2). To account for the simultaneous comparisons of n_m measured quantities with model predictions, the Šidák correction for multiple hypotheses testing [48] is applied in the calculation of threshold bounds in Eq. 2).

$$\forall i \in \{1, 2, ..., n_m\} : \phi_d^{1/n_m} = \int_{T_{low,i}}^{T_{high,i}} f_{U_{c,i}}(U_{c,i}) dU_c \quad (2)$$

A parameter combination instance is falsified if for one measured quantity the residual between model prediction and measurement, $g_i(\theta) - \hat{y}_i$, lies outside the interval delimited by the lower and upper thresholds. Model instances that have been falsified are assigned a probability of 0. *Candidate* models satisfy equation 3 for all n_m measured quantities and are assumed to be equally likely.

$$\forall i \in \{1, 2, ..., n_m\} : T_{low,i} \leq g_i(\theta) - \hat{y}_i \leq T_{high,i} \quad (3)$$

Rectangular regions of acceptance of residuals between model predictions and measurements provide candidate models that are robust with respect to unknown and changing correlations between residuals related to multiple measured quantities [38, 39, 49].

2.2. Physics-based model: The applied-element method

The proposed framework involves structural identification of the parameters of a physics-based model. Thus, parameter values of the physics-based model that are compatible with post-seismic evidence are inferred and subsequently used to perform behavior predictions that involve extrapolation. In this paper, the applied-element method (AEM) is used as physics-based model in order to simulate pushover curves (see Section 2.3). In addition, AEM provides a link between the reduction in fundamental frequency (as a consequence of damage) and the displacement at the top of the building. This means that for each displacement value of the pushover curve, the fundamental frequency of the building is determined, as discussed in Section 2.3.

AEM is a numerical modeling strategy that has been developed as an alternative simulation technique to the finite element method. AEM captures high geometric and material non-linearities. In order to capture a large range of failure modes that can be found in reinforced-concrete and masonry structures - such as rocking, joint de-bonding, sliding or shear diagonal cracking - the AEM divides structural components into small

elastic elements that are connected through springs as illustrated in Figure 2. Thus, elements do not share common points unlike finite elements, and this enables simulation of large displacements and progressive element separation through failure of the contact springs [50].

Pairs of normal and shear springs localize stresses, strains and deformations at the element contact points [51] (see Figure 2). The behavior of masonry blocks is assumed to be similar to concrete-type behavior models, described by a Maekawa compression model that includes unloading and reloading [52], as shown in Figure 2. Accordingly, the envelope of the compressive stress-strain behavior law is defined by the initial Young's modulus, the fracture parameter representing the extent of the internal damage, and the compressive plastic strain. Tensile stresses follow a linear behavior law up to the cracking point when tensile strength is reached. Thus, the material is assumed to crack when major principal stresses reach maximum tensile strength. Once cracked, the spring stiffness is set to be zero as the spring is modelled to be broken.

In shear, the tangent modulus is calculated according to the strain at the spring location. Shear stress and shear strain follow a linear relationship until cracking. Then, shear stresses drop to a level of shear stress that depends on the aggregate interlock and friction at the crack surface. Once separation strain is reached, adjacent elements are separated at the connecting face. All the springs are cut and, if the elements create contact again during further steps of the analysis, the contact behavior is similar to two rigid bodies. In case of contact between elements, linear springs are generated at contact points, governed by parameters such as normal and shear contact-stiffness factors and friction coefficient in case of contact between initially linked elements. When a material undergoes combined compressive and shear stresses, the failure of the material follows the Mohr-Column failure envelope.

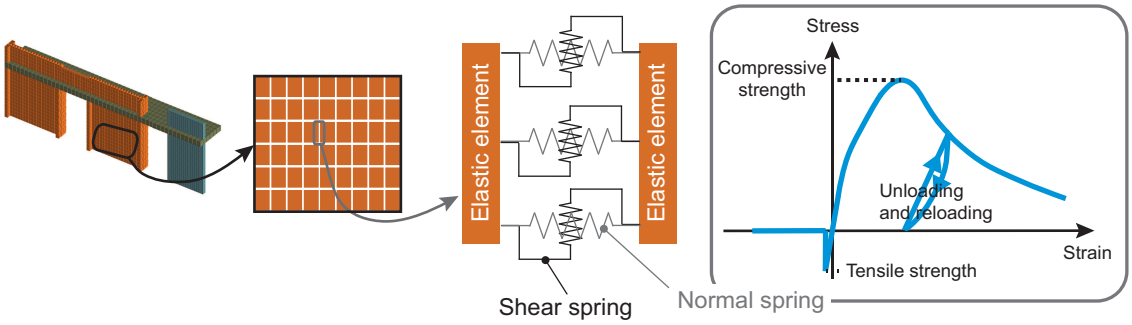

Figure 2: Principle of the applied-element method (AEM). Structures are divided into elastic cubes that are connected by pairs of nonlinear normal and shear springs. Masonry elements are simplified to have averaged behavior between mortar and masonry blocks.

Thus, springs defined by the AEM are able to capture joint de-bonding, shear sliding, direct tension and partial connectivity between elements. However, shear-compression failure due to high axial loads is not taken into consideration. AEM has been shown by several researchers [53, 54, 55, 56, 57, 58, 59, 60] to predict post-yield structural behavior of masonry and reinforced-concrete structures that are defined by a particularly large range of potential failure modes. The applicability of AEM to successfully simulate large

deformations has been demonstrated by Tagel-Din and Meguro [61], among others. In this paper a macro-modelling approach is chosen, in which bricks, mortar joints and brick-mortar interfaces are represented as an equivalent material. Such an approach is most suitable for practical applications of the AEM, especially when populations of models are simulated.

2.3. Static nonlinear predictions of seismic behavior

Static nonlinear pushover curves provide predictions of displacement capacities of buildings that are independent of earthquake excitation and therefore do not require earthquake-related information. Three-dimensional nonlinear models (such as AEM-based models described in the previous section 2.2) provide a link between top displacement (that can be related to DGs) and the reduction in natural frequencies due to damage, as shown in Figure 3. Figure 3 shows a pushover curve (base shear as a function of top displacement) and the DGs related to particular points of the pushover curve. In addition, Figure 3 shows the evolution (i.e. reduction) of the fundamental frequency as a function of top displacement. Nonlinear numerical models, that have localised formulations of influence of damage on stiffness, provide simulation results for both curves presented in Figure 3. Also, when such high-fidelity models are used, pushover-curve simulations present an interesting reduction in computation time when compared to full-transient dynamic time-history analysis for which calculation time - especially in a multiple-model setup - can become prohibitive.

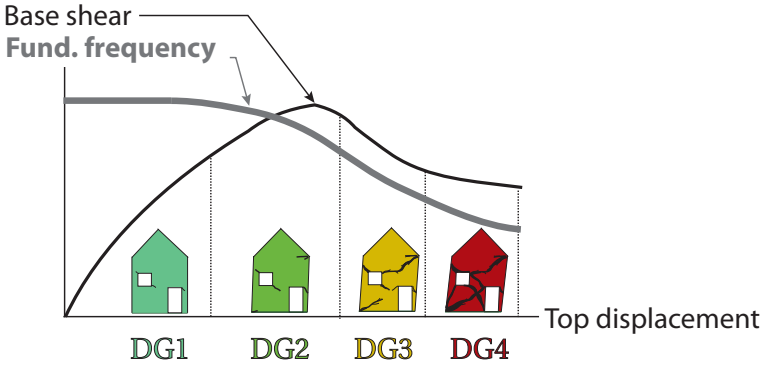

Figure 3: Schematic representation of the evolution of damage and natural frequency under increasing lateral top displacement, as typically simulated by pushover analyses.

Using for instance the N2 method proposed by Fajfar et al. [62], predictions of the displacement demand related to a given seismic demand (in the acceleration-displacement response spectrum (ADRS) format) can be made. Thus, displacement demands can be derived for a given building with respect to code-based seismic displacement-demand spectra or acceleration-displacement response spectra of real earthquakes. In the proposed framework, the goal is to predict vulnerability curves: evolution of predicted DGs with respect to increasing seismic demands. In order to simplify predictions, DGs are predicted with respect to changing earthquake levels that are expressed as peak ground acceleration (PGA) values. The same seismic demand spectrum is scaled in order to obtain increasing

PGA values (see Figure 4). Figure 4 contains an illustration of scaling (or magnifying) the demand spectrum to increasing amplitudes in order to derive, for the same pushover curve, the corresponding values of displacement demands and thus, predicted DGs.

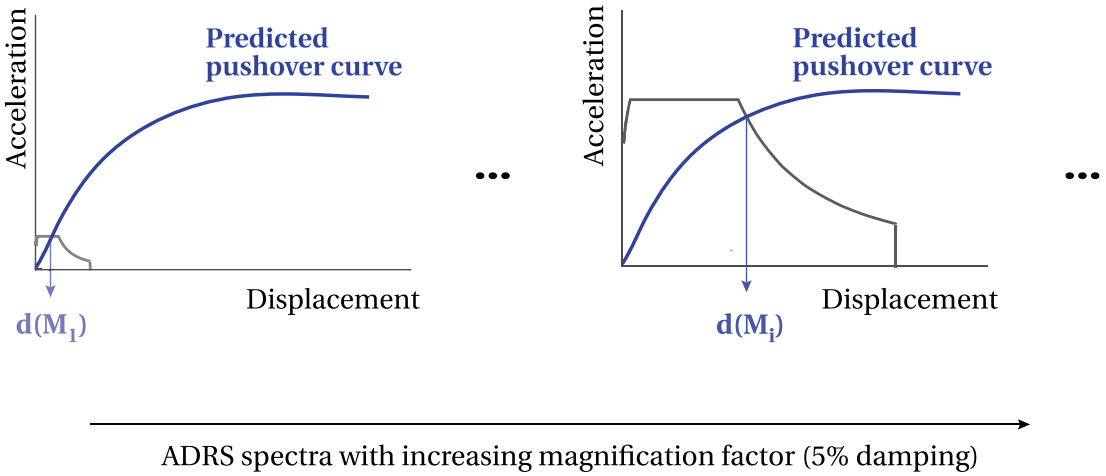

Figure 4: Predicting displacements for increasing demand M_i using simulated pushover curves and scaled design spectra in the acceleration-displacement response spectrum (ADRS) format.

A limitation of vulnerability predictions using pushover curves is related to the assumption of in-plane-collapse mechanisms. By enforcing a certain load distribution (often triangular displacement distributions along the building height or a displacement distribution that is similar to the mode shape of the fundamental mode), the collapse mechanism is often limited to in-plane load-bearing. For some buildings, this load-bearing mechanism is not realistic. Recently, adaptive pushover techniques have been proposed to overcome some of the aforementioned limitations [63, 64]. However, in the context of this paper, classic pushover curves are considered with triangular displacement distribution applied to the initial centre of torsion of the slabs. Relying to such pushover curves assumes that the building behavior under earthquake loads is dominated by the fundamental mode. As stated before, the scope of buildings for the proposed methodology is limited to shear-resisting buildings and thus, the conditions for use of pushover curves are expected to be met.

2.4. Combining visual inspection and ambient-vibration data

As mentioned in Section 2.3 a physics-based model is used to establish a link between displacement at the top of the building and reduction in natural frequencies (as a function of damage). Thresholds based on the measured post-earthquake frequency and the estimated combined uncertainty are subsequently used to derive for each model instance $g(\theta)$ the range of displacement demand (such as top displacement or first-story drift) that are compatible with frequency thresholds. The interval that is delimited by the displacement demand, $d_{f-drop,T_{high}}(\theta)$, corresponding to the upper threshold, T_{high}, and the displacement demand, $d_{f-drop,T_{low}}(\theta)$, corresponding to the lower threshold, T_{low}, is

denoted $\Delta_{f-drop}(\theta)$, as shown in Figure 5. Similarly, using thresholds on the observed DG_{VI}, an interval of potential values of displacement demand that are compatible with visually observed DGs can be derived. This interval is denoted $\Delta_{DG}(\theta)$ (see Figure 5).

Candidate parameter combinations, $\theta \epsilon \Omega''$, need to verify the condition that the subset of intersection between the displacement demand intervals defined by measured post-earthquake frequency, $\Delta_{f-drop}(\theta)$, and observed DG, $\Delta_{DG}(\theta)$, is not empty, as established by Equation 4 and illustrated in Figure 5. It is recalled that candidate models that are obtained using Equation 4, require no information regarding the ground motion or the initial building state.

$$\Omega'' = \{\theta \epsilon \Omega \mid \Delta_{f-drop}(\theta) \cap \Delta_{DG}(\theta) \neq \emptyset\} \tag{4}$$

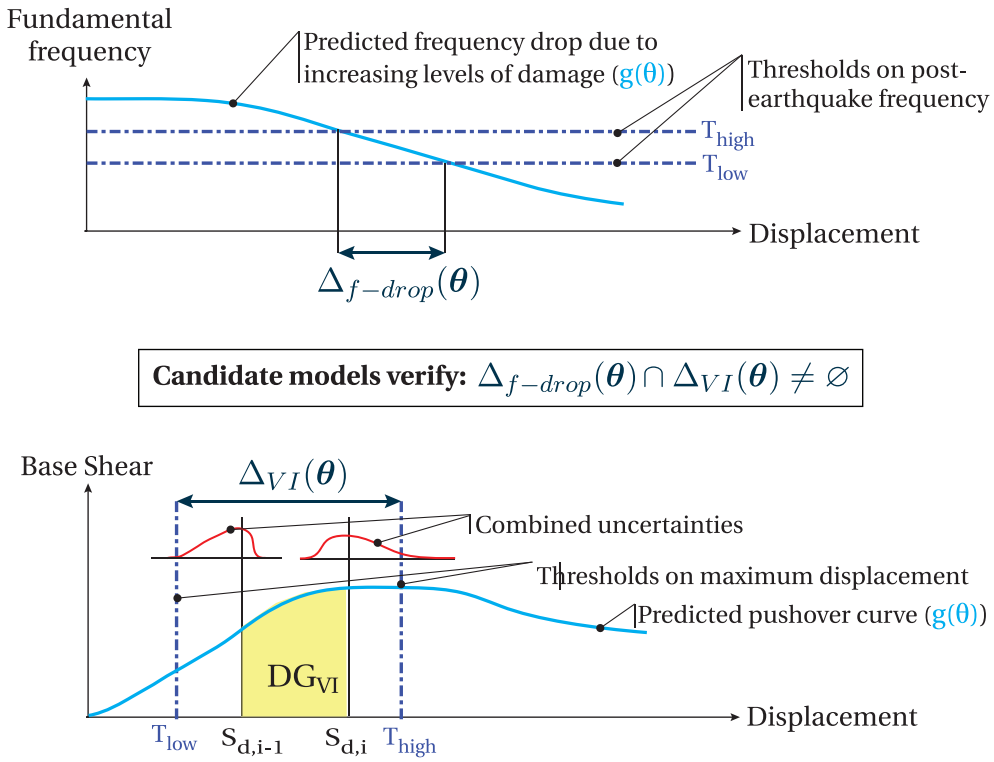

Figure 5: Post-earthquake structural identification based on static nonlinear predictions of frequency drop and base shear as a function of displacement demand. Candidate models have an intersection subset of displacement values between intervals based on measured frequency and observed DG.

2.5. Iterative introduction of measured information

The framework presented in Figure 1 is intended to be applied in an iterative and sequence-free manner. Therefore, two potential sequences of structural identification of earthquake-damaged structures are described in order to show the potential of the

proposed framework to incorporate new information sources and to adapt to the needs identified by the engineer, who is at the center of the framework (see Figure 1). The case study described in Section 3 will provide further insight into the applicability of the framework.

2.5.1. Structural-identification sequence example 1

Step 1 - In-situ inspection: After a damaging earthquake, visual screening (VS) of a building is performed in order to determine the DG and to exclude dangerous collapses of non-structural elements.

Step 2 - Ambient-vibration measurements: Using one sensor (typically at the top of the building) the fundamental frequency in each direction can be derived.

Step 3 - Developing a model: From VS or from construction drawings a physics-based three-dimensional model is developed.

Step 4 - EDMF: Predictions of an initial model population of the physics-based model (based on combinations of parameter values) are compared to the measured natural frequency (using Eq. 3) after estimating the ranges of uncertainties that arise from measurement and modelling errors. The whole model population is falsified, indicating either a wrong modelling assumption or misevaluated uncertainties. It is the role of the engineer to decide which task(s) of the framework (see Figure 1) should be re-evaluated.

Step 5 - Detailed in-situ inspection: Given the complete model population is falsified an in-depth visual inspection of the damaged building is performed to detect model assumptions that are not compatible with the selected model. A slight soil-structure interaction is observed as well as cracks in the floor-slabs that fail to provide complete redistribution of the forces between the walls.

Step 6 - Redefining uncertainties: Uncertainty bounds are redefined (increased) in order to include the observations from the detailed in-situ inspection.

Step 7 - EDMF: Based on the new uncertainty distribution, EDMF is performed again without the need for resimulation of the physics-based model. A large range of candidate models is found which undermines prediction precision. Again, several tasks of the framework (see Figure 1) can potentially be re-evaluated.

Step 8 - Refining the model: The physics-based model is refined in order to include the outcomes of the in-depth visual inspection (Step 5) and new simulations are performed.

Step 9 - EDMF: Based on the initial uncertainty distribution (Step 4), EDMF is performed again. An acceptable number of candidate models is obtained and the prediction uncertainty is deemed acceptable by decision-makers (typically parametric uncertainty on predictions is of the same order of magnitude than modelling uncertainties).

Step 10 - Prognosis: The vulnerability prediction of the deteriorated structure exceeds minimum requirements set by decision-makers. Therefore, the residual capacity is estimated to be insufficient and the building is tagged unsafe for occupancy. The candidate model instances found in Step 9 are thus kept in order to estimate the utility of repair interventions.

2.5.2. Structural-identification sequence example 2

Steps 1 to 3 : Similar to example 1.

Step 4 - EDMF: Model-population predictions are compared to measured evidence (using Eq. 3). Falsification performance is poor and parametric uncertainty remains too

high for objective decision-making and thus, the engineer needs to re-evaluate one or more tasks of the iterative framework (see Figure 1).

Step 5 - Estimating expected utility of additional measurements: The physics-based model is used to estimate the expected utility of additional measurements such as mode-shapes (requiring an array of sensors) or laboratory tests on a given material type. It is concluded that the expected utility of such measurements is low.

Step 6 - Information from city-scale comparisons: In order to retrieve additional sources of information, the engineer decides to perform city-scale comparisons. For instance, a building that is of a similar building class and shows no signs of damage can be used (with increased modelling uncertainty) as an estimate of the initial (undamaged) natural frequency. In addition, based on the candidate models, a rough estimate of the amplitudes of the response spectrum of the main-shock can be obtained.

Step 7 - EDMF: Based on the new sources of measurements obtained in Step 6, EDMF is performed again. Falsification performance is increased and thus, performance predictions are performed.

Step 8 - Prognosis: The predicted vulnerability of the deteriorated structure complies with minimum requirements that are set by authorities. Upon verification that no secondary (non-structural) elements are a source of danger for the inhabitants, the building is tagged safe for occupancy.

3. Case study

The methodology is applied to a case study in order to illustrate applicability and potential of model-based data interpretation with scarce measurement data to enhance building-state-related knowledge. The case study is a half-scale mixed unreinforced-masonry reinforced-concrete building with four floors see Figure 6) that has been tested on a shake table under an earthquake sequence with increasing amplitudes of shaking by Beyer et al. [65]. Schematic building drawings of the tested specimen are provided in Figure 6. Additional masses have been added to the slabs in order to comply with similarity laws for stresses.

The earthquake excitation that has been used during the shake-table tests is the east-west component measured at the ground station of the Ulcinj-Hotel Albatros station during the April 15th, 1979 Montenegro earthquake [66]. This accelerogram has a reasonable match with a slightly modified version of the Eurocode 8 spectrum for soil class D (see [65] for further details regarding the design spectrum).

Shake-table tests exclude uncertainties from environmental influences (such as temperature, irradiation and changing soil conditions). In addition, no non-structural elements such as separation walls and windows influence the natural frequencies. Finally, the applied accelerations have been unidirectional in the longitudinal direction, reducing torsional and bi-directional effects. Since the level of uncertainties of this case-study is low, identification and prediction results represent upper bounds to the performance of the proposed methodology. Nevertheless this case is of interest because ambient-vibration data on a building under a sequence of earthquake events and for multiple damage states is scarce, especially for European building types (low-rise mixed masonry-concrete buildings). In addition, the shake-table tests comparisons of predictions with observed behavior of structures under subsequent shaking events.

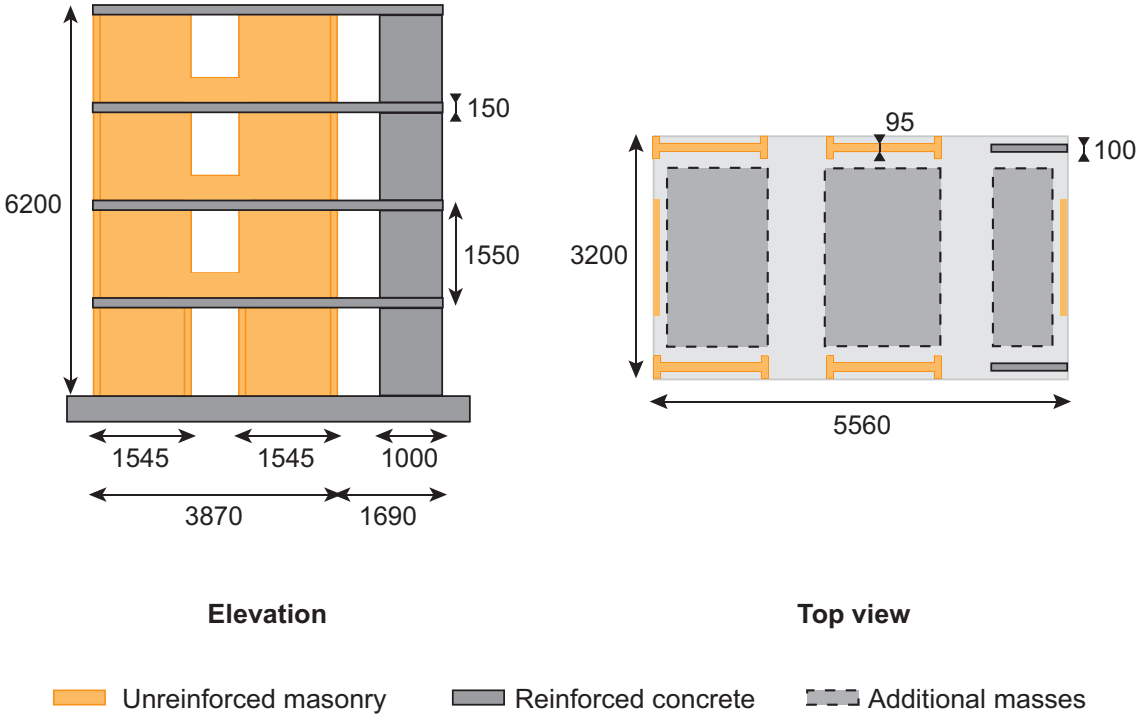

Figure 6: Schematic drawings of the mixed unreinforced-masonry reinforced-concrete building tested on a shake table by [65]. Dimensions correspond to a half-scale specimen. Additional masses have been added to comply with similarity laws for stresses. Shake-table tests have been uni-directional in the longitudinal direction.

3.1. Relation between structural damage and fundamental frequency

White-noise (WN) excitation has been tested between shake-table tests [65] and the findings are summarized in Table 1 for the building states after shaking events 3 to 8 (no WN tests have been carried out between shaking events 6 and 7). The initial (undamaged) fundamental frequency of the building has been measured to be 7.9 Hz. The DG observed following the tests vary from DG1 to DG3. As can be seen in Table 1 the amplitudes of vibration exceed the levels of ambient vibrations, for which a range of $1\,\mu m\,s^{-2}$ to $1\,mm\,s^{-2}$ is generally admitted. In addition, for the white-noise tests following shaking event 5, the amplitude of shaking is of one order of magnitude lower compared to the other tests. Thus, higher values of fundamental frequencies are obtained. This is in agreement with previous observations [67] and can be explained by an elastic reduction of stiffness under higher amplitudes of shaking.

When comparing WN tests that involve similar amplitudes of shaking (Tests 3, 4, 7 and 8 in Table 1), a trend of frequency-reduction with increased levels of damage (higher DGs) can be observed (for the first two fundamental frequencies in the longitudinal direction, f_1 and f_2). This tendency is a necessary starting point for the proposed methodology. Previous research [11, 9] has resulted in the conclusion that a frequency drop of approximatively 30% is the limit of DG1. In this case-study, the boundary seems

to be lower, as DG2 is observed for a frequency drop of less than 30% (see Table 1). This difference may have arisen from the laboratory conditions, where the pre-stressed anchorage of the building to the shake table remain elastic and no reduction of soil stiffness from large-amplitude vibrations occurs.

Table 1: Influence of observed damage on the measured natural frequencies.

Test	f_1 [Hz]	Reduction f_1 [%]	f_2 [Hz]	AV level [mm/s^2]	DG
3	6.6	-16.5	24.1	176	1
4	5.8	-26.6	23.8	176	2
5	6.3	-20.3	23.9	26.2	2
7	5.3	-33.0	23.2	175	2
8	5	-37.0	21.6	176	3

3.2. Physics-based model using the applied element method

A three-dimensional model using the applied-element method (AEM) (see Section 2.2) is build to predict nonlinear structural behavior. Unreinforced masonry is modelled as nonlinear macro-elements in a similar way to concrete elements. The numerical model is in total composed of 27′552 elements connected by 1′718′587 nonlinear springs.

Given uncertainties on density are comparatively low, only material parameters related to load-resisting properties are included in the analysis. The load-resisting material properties that apply to both masonry and concrete elements are: Young's modulus, Poisson's coefficient, maximum strain, friction coefficient as well as maximum tensile and compressive strengths. Thus, 12 parameters are identified to influence the nonlinear lateral load-bearing behavior of the modelled building. The 12 parameters, along with the range of values that is assumed based on engineering judgement and existing literature are reported in Table 2. Although steel reinforcement bars have an influence on the predicted pushover curve and especially the predicted ultimate displacement, these structural elements do not have a significant influence on the fundamental frequency and therefore, standard reinforcement is assumed throughout the analysis.

Pushover curves of the studied building are obtained by enforcing a triangular lateral displacement shape at the centre of torsion of the four slabs. The obtained pushover curves characterise the total shear force at the base of the building as a function of top displacement. As the exact definition of yield displacement based on simulated cracks is time consuming and uncertain [68], a bilinear approximation of the predicted pushover curve is derived through minimizing the error between the AEM-based curve and a bilinear approximation. The yield displacement is subsequently derived from the bilinear curve. In addition, a global definition is used to derive ultimate displacement which is reached when the total base shear force drops below 80% of the maximum base shear. Such global definitions carry some uncertainty but are necessary for automated prediction of yield and ultimate displacement in a model-population approach.

A sensitivity analysis using a Box-Behnken design-of-experiment scheme [69] is performed in order to assess the relative importance of each parameter on the prediction results. The prediction results that are used to derive the relative importance are yield displacement, ultimate displacement, initial frequency and frequency after 6 mm of top displacement. Using linear regression, an estimate of the sensitivity values is obtained

Table 2: Parameters included in the sensitivity analysis (Box-Behnken design of experiments). The five parameters with the highest influence on yield displacement (d_{yield}), ultimate displacement (d_{ult}), initial fundamental frequency (f_{ini}) and fundamental frequency at $6mm$ top displacement (f_{6mm}) are retained as primary parameters for the analysis.

Parameter	Units	Range	Sensitivity [%]				Retain
			d_{yield}	d_{ult}	f_{ini}	f_{6mm}	
Masonry							
Young's mod.	kN/mm^2	[2,8]	37	35	71	51	Yes
Poisson's coeff.	-	[0.1,0.3]	1	3	5	0	No
Maximum strain	mm/m	[0.5,8]	0	7	0	0	No
Friction coeff.	-	[0.6,0.8]	7	9	0	1	No
Tens. strength	N/mm^2	[0.05,1.5]	19	22	2	25	Yes
Compr. strength	N/mm^2	[4,12]	8	11	0	4	Yes
Reinforced Concrete							
Young's mod.	kN/mm^2	[20,40]	20	5	20	8	Yes
Poisson's coeff.	-	[0.1,0.3]	2	0	1	1	No
Maximum strain	mm/m	[1,10]	0	0	0	0	No
Friction coeff.	-	[0.7,0.8]	1	1	0	0	No
Tens. strength	N/mm^2	[1,3]	5	6	0	10	Yes
Compr. strength	N/mm^2	[30,50]	0	0	0	1	No

and reported in Table 2. Although the precise choice of the value of 6 mm is arbitrary, it ensures slight damage for all parameter combinations. Changing the displacement value taken for sensitivity analysis in the range of slight damage does not significantly alter the conclusions of the analysis and thus, the parameters selected as primary parameters do not change. Young's modulus of masonry is found to have the highest influence on all predictions.

Parameter selection for the subsequent model-based data interpretation using EDMF is based on the following criteria: a relative importance exceeding five percent on two predicted values and on average on the four predicted values. Thus, five parameters are retained to build the initial model population using grid sampling (see Table 2): Young's modulus of masonry (4 divisions), tensile strength of masonry (3 divisions), compressive strength of masonry (2 divisions), Young's modulus of concrete (3 divisions) and tensile strength of concrete (2 divisions). In total, the initial model population is composed of 144 model instances. The vulnerability prediction that is obtained using the 144 parameter combinations of the initial model population (no data interpretation is done) and the estimated uncertainties (see Section 3.3.1) is shown in Figure 7. A Monte-Carlo combination of predictions using static nonlinear predictions and the N2 method for scaled spectra is used (see Figure 5).

3.3. Model-based data interpretation using sparse measurements

As explained in Section 2.4, DGs oberved using visual inspection and post-earthquake fundamental frequencies derived from vibration measurements are combined to reduce parametric uncertainty related to an earthquake-damaged building. The EDMF methodology is applied to falsify model instances that are not compatible with observed evidence.

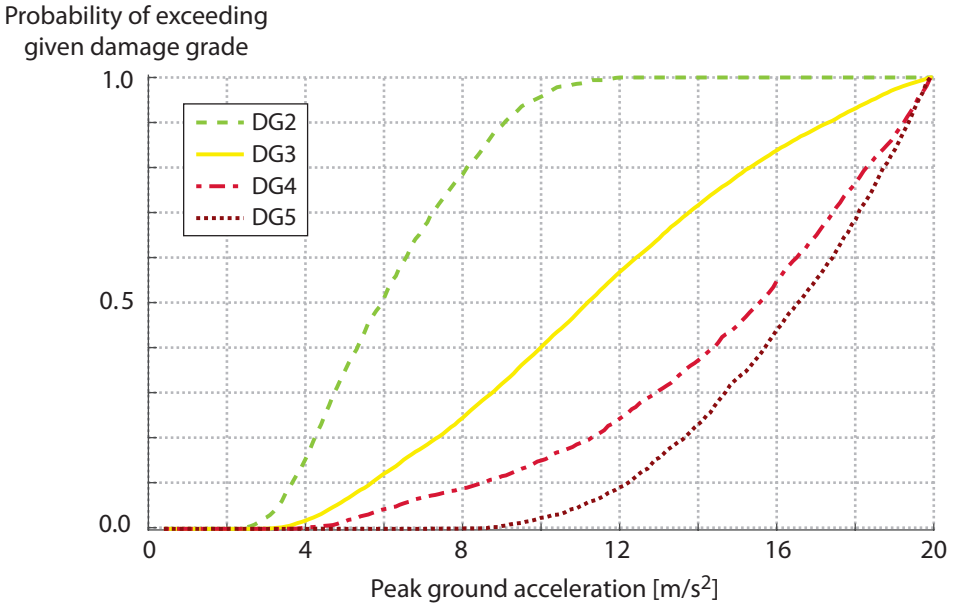

Figure 7: Initial vulnerability predictions (prior to earthquake shaking and without considering measurement data) using scaled acceleration-displacement spectra following the static nonlinear approach (see Figure 5).

3.3.1. Sources of uncertainty for identification

An important step of the EDMF methodology, which is used to interpret measurement data, is related to estimated uncertainties that influence measured and observed behavior. For the measurements and model predictions used in the case study, the following uncertainty sources are detected and estimated based on engineering judgement (previous work has shown that EDMF is robust with respect to uncertainty estimates [40]):

- A *measurement uncertainty* resulting from sensor precision, weather and loading conditions as well as time-domain to frequency-domain transformation is estimated to follow a zero-mean normal distribution with a standard deviation of 0.15 Hz.
- A *model uncertainty* in predicting the natural frequency is estimated to be part of the interval $[-0.08, 0.04]$. Given the reduction in natural frequency is obtained by loading-only (instead of loading-unloading) the model prediction is predicted to be biased towards lower values. Given the lower level of amplitudes that characterize WN excitation after shaking event 5, the uncertainty interval is changed to $[-0.12, 0.0]$, as the model does not predict regaining higher stiffness values under very low shaking amplitudes.
- A DG boundary *definition uncertainty* is estimated to result from subjectivity in visual inspection and from the empirical definition of the DGs as well as model imprecisions in displacement predictions. The estimated relative uncertainty range

for the DG boundaries is: $[-0.125, 0.125]$ for $S_{d,1}$; $[-0.25, 0.25]$ for $S_{d,2}$ as well as $S_{d,3}$; and $[-0.20, 0.05]$ for $S_{d,4}$.

3.3.2. Performance of structural identification with scare measurements

Using Equation 4, model instances that have incompatible ranges for displacement demand between the observed DG and the measured fundamental frequency are falsified. Using this sparse post-earthquake information sources, the performance of model falsification is estimated using the reduction in model instances (i.e. the percentage of initial model instances that is falsified), which is an indirect performance indicator. For the post-shaking situations summarised in Table 1, 75% of the initial model instances are falsified after shaking event 3, 57% after shaking event 4, 53% after shaking event 5, 63% after shaking event 7 and 17% after shaking event 8. Thus, based on these performances the observed DG influences the performance of EDMF in this specific case. In other words, the initial model population generally predicts higher DGs compared to the observed DGs for a given frequency drop.

In Figure 8 a parallel-axes plot provides an overview of the identification results using data following shaking event 5. The parallel axes allow for presentation of normalized ranges of parameters and predictions. Given the parameter space is sampled using grid sampling, the five first vertical axes that contain parameter values in Figure 8 have equidistant values (that are unchanged after falsification), while prediction values show a larger scatter. Although no reduction in the range of parameters is obtained, 53% of the initial model population is falsified as stated before. The reduction in model population results from falsifying several parameter combinations. This results in a reduction of the prediction range of yield displacement of 77%. Reduction in uncertainty of initial frequency and ultimate displacement remains low compared to the uncertainty reduction regarding yield displacement, as can be seen in Figure 8. Therefore, adding information on initial frequency, as proposed in the iterative framework has potential to further decrease parametric uncertainty.

Table 3: Performance of model-based measurement identification with scarce measurements following five shaking events.

Event nr	Falsified instances [%]	Yield displacement range reduction [%]	Ultimate displacement range reduction [%]
3	76	13	3
4	60	12	3
5	62	60	2
7	65	14	2
8	18	3	3
4 and 5	71	38	35
5 and 7	81	50	35

Given the iterative nature of the proposed framework, falsification can be performed for two consecutive shaking events without additional model-simulation runs. Thus, when information obtained following shaking events 4 and 5 are combined 71% of the initial model population are falsified, whereas 81% are falsified by combining information obtained after events 5 and 7 (see Table 3).

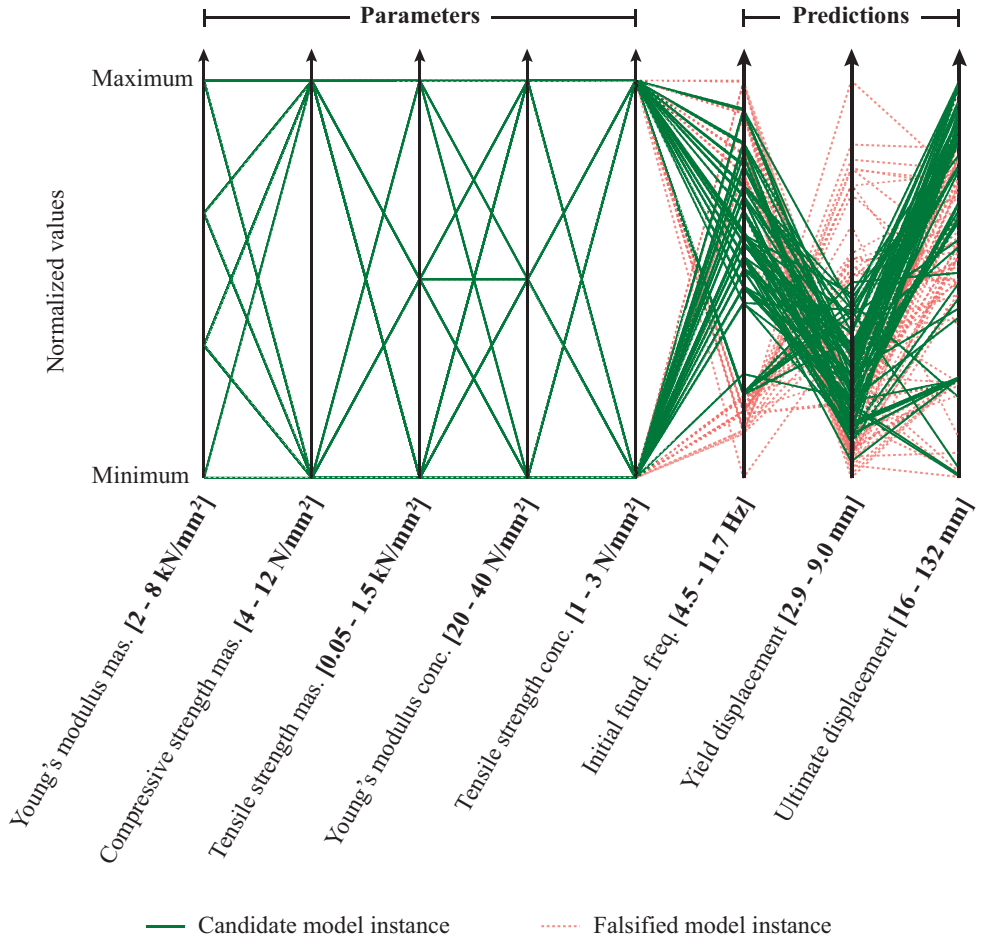

Figure 8: Parallel axes plot showing the results of model falsification using data following shaking event 5. The first five parallel axes contain normalized parameter ranges and the last three parallel axes contain normalized prediction values of the initial fundamental frequency, yield displacement and ultimate displacement. While little reduction in the parameter ranges is obtained, prediction ranges (especially yield displacement) are reduced.

3.4. Predicting structural vulnerability during subsequent shaking

Using the candidate models that are obtained using model-based measurement interpretation as described in the previous Section 3.3.2, the vulnerability of the building with respect to future shaking events is predicted using the prediction methodology described in Section 2.3. For predictions, the initial slope of the pushover curve is replaced with the fundamental frequency derived from vibration measurements after the previous shaking up to the intersection of the deteriorated slope with the initial pushover curve.

3.4.1. Sources of uncertainty for predictions

Similarly to the identification step, several sources of uncertainty affect the model predictions based on pushover curves using the N2 method. A relative uncertainty following a zero-mean normal distribution with a standard deviation of 7.5% is linked to the acceleration demand values given by the ADRS spectra. The base-shear values are estimated to be affected by a uniform relative uncertainty bounded between -20% and 20%, which also covers uncertainty related to the N2 method itself, which has been shown to be inaccurate for high frequency values when the equal displacement rule does not apply [70]. For the uncertainties related to the definition of DG boundaries the same values than for identification are used (see Section 3.3.1).

The initial slope of the pushover curves is given by the fundamental frequency that is measured after the previous earthquake. This fundamental frequency is estimated to have a biased uncertainty taken from the interval $[-0.10, 0.0]$ when displacement demand is predicted using the N2 method. This uncertainty is not related to measurement uncertainty (which is typically centered on zero). The uncertainty arises from the physics-based model not capturing the elastic frequency drop (nonlinear elasticity) that structures exhibit under large-amplitude vibrations [10]. In addition, this frequency drop cannot be exactly known and varies between buildings. The uncertainty is biased towards negative values, as buildings always show elastic frequency drops and never an increase in frequency. In classical assessment approaches, such frequency drops are explained by reducing the modulus of elasticity of building materials.

In applications based on real ambient vibrations this uncertainty would be even more biased towards negative values, as suggested by Michel et al. [67], who found an elastic frequency drop close to 33%. As the WN tests following shaking sequence 5 involves much lower lower amplitudes of vibration (see Table 1), the uncertainty interval is thus estimated to be more biased: $[-0.15, 0.5]$. All the described uncertainty sources are combined with the parametric uncertainty of the candidate model set using a Monte-Carlo combination scheme with 50000 randomly selected samples.

3.4.2. Vulnerability prediction results using updated parameter values

The vulnerability prediction for the building state following shaking event 3 is shown in Figure 9. The cumulative density function of DGs 2 to 5 as a function of PGA allows the decision makers to take actions with enhanced knowledge regarding the safety for occupancy of the earthquake-damaged building. Compared with the initial vulnerability predictions (see Figure 7) the damage suffered by the building and the reduction in parametric uncertainties results in a more pessimistic prediction, mostly for DGs 1 to 3. As can be seen in Figure 8, the reduction in uncertainty is more important for yield displacement than for ultimate displacement and thus, the prediction for DGs 4 and 5 is less affected. This is also due to the fact that in this example, a DG 1 has been observed. In the following shaking event 4 (PGA equal to $3.5\,\mathrm{m\,s^{-2}}$), a DG2 has been observed. This observed behavior is predicted with a probability of 65%. In comparison with the initial vulnerability predictions without measurement interpretation (see Figure 7) the vulnerability prediction carries less uncertainty and ambiguity. In addition, the initial vulnerability curve inaccurately predicts a DG1 with more than 95 percent probability - showing potentially unsafe predictions when damage is not taken into account and no structural identification is performed.

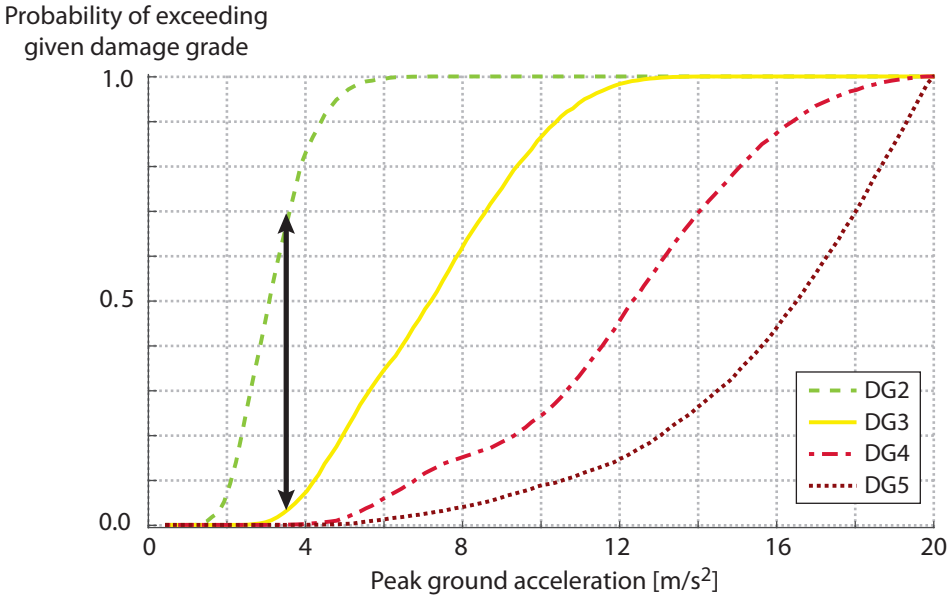

Figure 9: Vulnerability prediction using scaled acceleration-displacement spectra (see Figure ref-fig4:DisplacementDeltaIdentification) based on candidate models that are identified using data available after shaking event 3. The arrow indicates the DG 2 observed for the following shaking event 4.

The vulnerability prediction for the building state following shaking event 7 is shown in Figure 10. In the following shaking event 8 (PGA of $6.4\,\mathrm{m\,s^{-2}}$), a DG3 has been observed. This observed behavior is predicted with a probability of 55%. In a similar way, Figure 11 gives the vulnerability prediction for the building state following shaking event 8. The DG 4 to 5 observed during the subsequent shaking test (PGA of $15\,\mathrm{m\,s^{-2}}$) is predicted with a probability of 100%. For the model-based measurement interpretation following the shaking events 4 and 5 the DG2 that has been obeserved during the subsequent test sequence are predicted with respectively 88% and 51%. These prediction results are obtained using exclusive post-earthquake observations from one building state. For all five building states used for model-based measurement interpretation, the observed DG of the following shaking test is predicted with a probability exceeding 50%, which is an encouraging result.

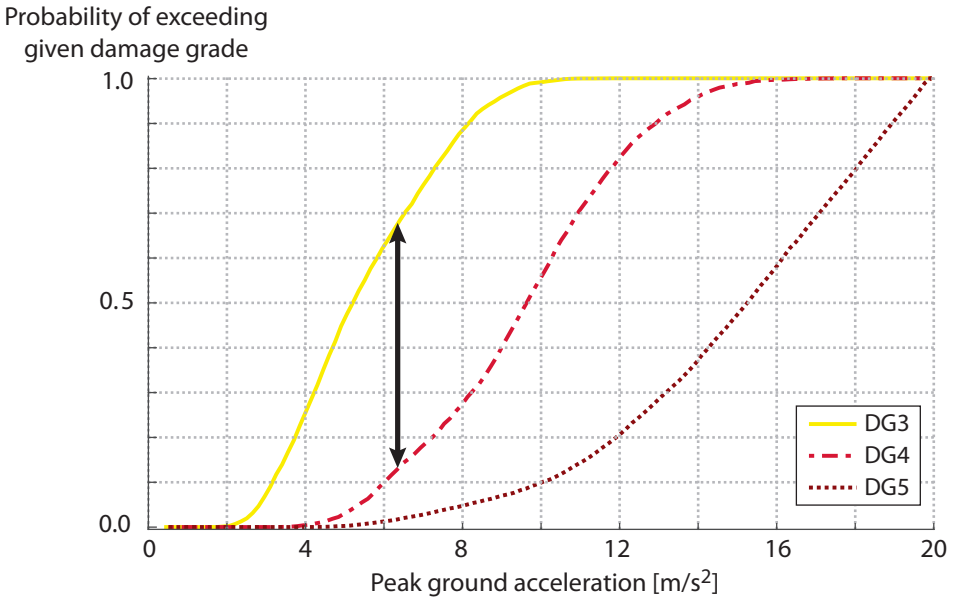

Figure 10: Vulnerability prediction using scaled acceleration-displacement spectra (see Figure 5) based on candidate models identified after shaking event 7. The arrow indicates the DG 3 observed for the following shaking event 8 (PGA = $6.4\,\mathrm{m\,s^{-2}}$).

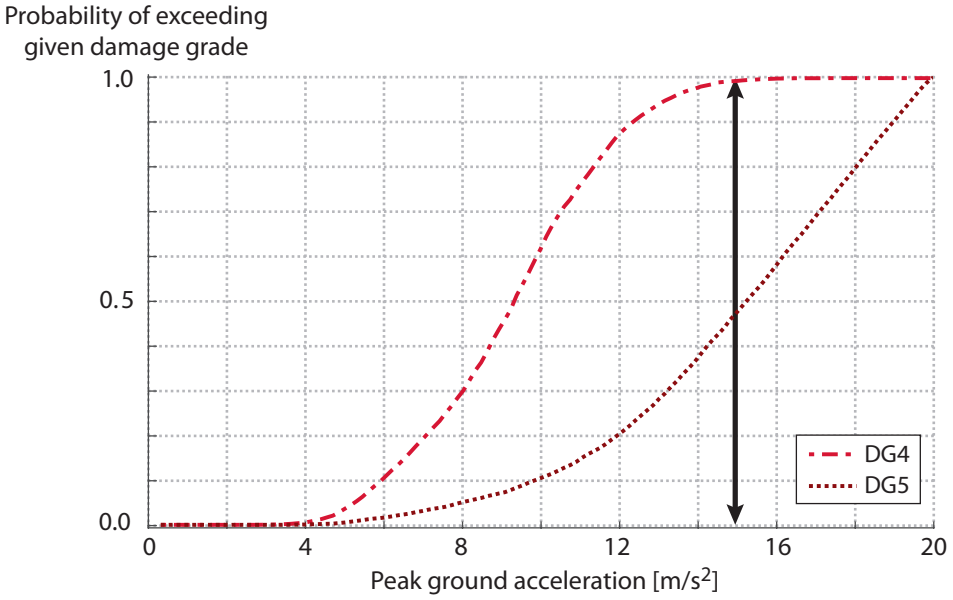

Figure 11: Vulnerability prediction using scaled acceleration-displacement spectra (see Figure 5) based on candidate models identified after shaking event 8. The arrow indicates the DG 4-5 observed for the following shaking event 8 (PGA = $15\,\mathrm{m\,s^{-2}}$).

3.5. Iterative identification during earthquake sequences

Earthquakes are rarely limited to a single shaking event, they often consist in a sequence of several shaking events or at least several aftershocks following a main shock. Using the candidate models that are identified following an earthquake event, not only classic vulnerability curves can be predicted (such as shown in Section 3.4), but also a prognosis can be made for the frequency drop related to given DGs that could be observed under subsequent shaking events. Such a prediction is shown in Figure 12 for the building state following shake sequence 7. In Figure 12 for each DG the probability distribution with respect to the amplitude of shaking (PGA) and the frequency drop is shown. With such a representation, approximate knowledge of the PGA of a subsequent shaking event allows the engineer to derive the most likely DG rapidly assess the utility of taking new vibration measurements (before taking measurements). Therefore, such predictions comply with the proposed framework (see Figure 1) as it guides the engineer in choosing the next iteration in case of aftershocks. As can be observed in Figure 12, in case of a earthquake that has a PGA of approximately $6\,\mathrm{m\,s^{-2}}$ (as is the case for the following shaking test, represented by a cross in Figure 12), the probability is spread mostly between 4 Hz and 5 Hz in case of a DG3. Therefore, the utility of taking additional measurements is limited, given the uncertainty related to fundamental frequencies.

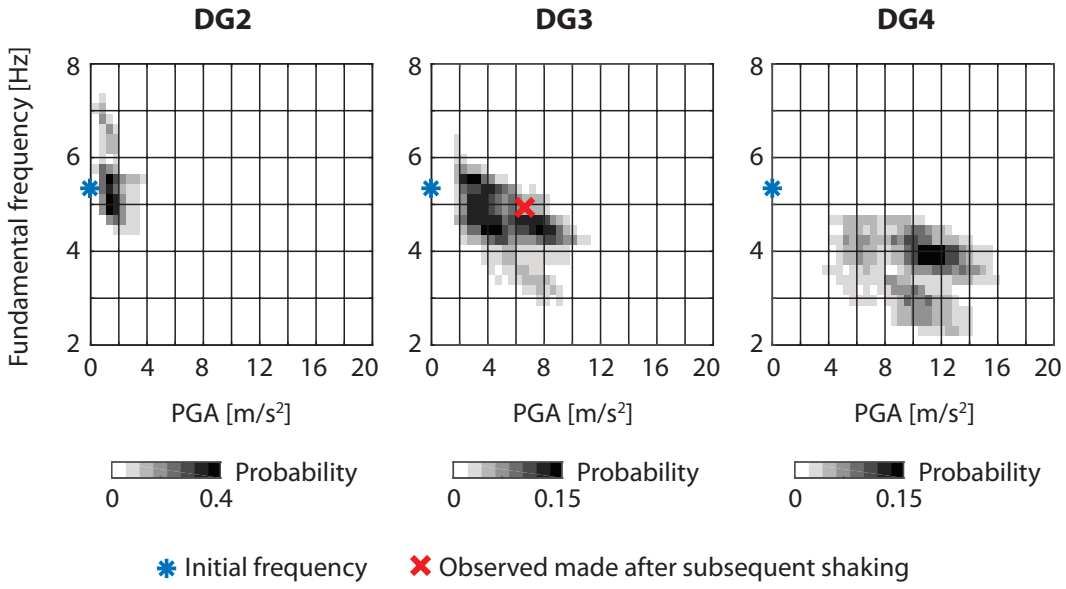

Figure 12: Prediction of the evolution of the fundamental frequency as a function of the amplitude of shaking (given in peak ground accelerations) for DGs 2 to 4, based on candidate models. Predictions are based on the building state after shaking event 7 and thus, the initial frequency corresponds to the natural frequency measured after shaking event 7 (5.3 Hz). The presence of fundamental frequency values exceeding the measured initial frequency is explained by accepting frequency values between thresholds and thus, exceeding the initial frequency (see Section 3.3.1. The cross indicates the observation made after the subsequent shaking event 8. Such predictions are a useful tool for rapid evaluation following an aftershock and gives an indication of the usefulness of additional vibration measurements.

4. Discussion

The proposed methodology of model-based interpretation of scarce post-earthquake measurements is applied to a shake-table structure, which has several limitations. As already discussed, the uncertainties from soil-structure interaction and secondary elements can be neglected in laboratory conditions. However, techniques exist to decouple modal properties of soil and structures [10]. Also, the earthquake signals are relatively close to the selected spectrum, which reduces uncertainties in the displacement-demand prediction.

In this paper, the methodology is applied to a single building specimen to illustrate applicability. General applicability of the methodology cannot be confirmed. It is anticipated that for full-scale in-service buildings, mass and stiffness contributions from non-structural elements are an important uncertainty source. In case of shear-resisting buildings, such as presented in the case study, the influence of structural elements has a more prominent influence than in case of moment-resisting reinforced-concrete frames with masonry infill walls. In cases of significant contribution from non-structural elements to global stiffness and mass of a building, major non-structural parts need to be modelled (as nonlinear elements) alongside structural elements, since damage to these elements can reduce natural frequencies of a building. If such elements cannot be modelled satisfactorily, the applicability and performance of the method are likely to be lowered.

The proposed methodology applies to buildings that show reduction in stiffness (cracks) prior to failure. In addition, the failure modes that are activated need to have a measurable influence on stiffness and thus, natural frequencies. Failure modes that do not have these characteristics (such as loss of bond between concrete and reinforcement bars) need to be investigated using alternative assessment tools.

Although the methodology is primarily intended for regions with low-to-medium seismic hazard, it can also be applied to regions with higher seismic hazard. As no information regarding the earthquake and the initial building condition is needed in this approach, the influence of previous damage (due to long-term degradation under successive earthquakes) is expected to have a marginal influence on the identification results. However, future work is needed to confirm when this is, and is not, true.

The methodology can also be applied using acceleration-displacement response spectra of true earthquake signals. Further research is needed to evaluate the applicability of the N2-method techniques to derive the displacement demand from inelastic spectra of real earthquakes (such as the equal-displacement rule).

5. Conclusions

A framework for model-based measurement interpretation in a post-earthquake context with scarce measurement information is proposed. This framework applies to shear-resisting buildings that show stiffness degradation prior to failure. In absence of baseline information related to the building and information regarding the signal and amplitude of the damaging earthquake, a three-dimensional nonlinear model is used to predict structural vulnerability of an earthquake-damaged shear-resisting concrete or masonry building. The work presented in this paper leads to the following conclusions:

- The framework allows engineers to reduce parametric uncertainties using scarce measurement data and perform accurate vulnerability predictions. DGs observed

during earthquake events following structural identification are predicted with probabilities of 50% to 100%. Between 13 to 76 percent of the initial model instances are falsified using observed DG and fundamental post-earthquake frequency. For these calculations no baseline information of the initial building state or the earthquake is needed.

- Error-domain model falsification (EDMF) is a suitable data-interpretation tool to combine measurement data from qualitative and quantitative sources. Potential displacement ranges that are compatible with measured post-earthquake fundamental frequencies as well as the observed damage grade are compared in order to discard inappropriate combinations of structural parameters.
- EDMF supports iterative integration of information and is thus compatible with decision-making processes in post-earthquake scenarios.

Acknowledgements

The authors acknowledge Prof. K. Beyer from the Earthquake Engineering and Structural Dynamics Laboratory, EPFL, for providing the test results. The authors thank Dr L. Diana for critical comments that helped improve the quality of the paper. This work was funded by the Swiss National Science Foundation under Contract No. 200020-169026.

References

[1] B. Galloway, J. Hare, D. Brunsdon, P. Wood, B. Lizundia, M. Stannard, Lessons from the Post-Earthquake Evaluation of Damaged Buildings in Christchurch, Earthquake Spectra 30 (1) (2014) 451–474.

[2] S.-L. Lin, S. Uma, A. King, Empirical Fragility Curves for Non-Residential Buildings from the 2010-2011 Canterbury Earthquake Sequence, Journal of Earthquake Engineering (2017) 1–29.

[3] D. A. McEntire, J. Cope, Damage Assessment After the Paso Robles, San Simeon, California, Earthquake: Lessons for Emergency Management, Natural Hazards Center, 2004.

[4] J. D. Marshall, J. C. Barnes, N. C. Gould, K. Jaiswal, B. Lizundia, D. B. Swanson, F. Turner, Post-Earthquake Building Safety Assessments for the Canterbury Earthquakes, in: Structures Congress 2012, 2012, pp. 1057–1068.

[5] L. Chiaraluce, R. Di Stefano, E. Tinti, L. Scognamiglio, M. Michele, E. Casarotti, M. Cattaneo, P. De Gori, C. Chiarabba, G. Monachesi, et al., The 2016 central italy seismic sequence: A first look at the mainshocks, aftershocks, and source models, Seismological Research Letters 88 (3) (2017) 757–771.

[6] M. Reyners, Lessons from the Destructive Mw 6.3 Christchurch, New Zealand, Earthquake, Seismological Research Letters 82 (3) (2011) 371–372.

[7] M. Basseville, L. Mevel, M. Goursat, Statistical model-based damage detection and localization: subspace-based residuals and damage-to-noise sensitivity ratios, Journal of Sound and Vibration 275 (3) (2004) 769–794.

[8] C. Gentile, A. Saisi, Ambient vibration testing of historic masonry towers for structural identification and damage assessment, Construction and Building Materials 21 (6) (2007) 1311–1321.

[9] F. Vidal, M. Navarro, C. Aranda, T. Enomoto, Changes in dynamic characteristics of Lorca RC buildings from pre-and post-earthquake ambient vibration data, Bulletin of Earthquake Engineering (2013) 1–16.

[10] A. Astorga, P. Guéguen, T. Kashima, Nonlinear elasticity observed in buildings during a long sequence of earthquakes, Bulletin of the Seismological Society of America 108 (3A) (2018) 1185–1198.

[11] F. Dunand, Y. Ait Meziane, P. Guéguen, J.-L. Chatelain, B. Guillier, R. Ben Salem, M. Hadid, M. Hellel, A. Kiboua, N. Laouami, et al., Utilisation du bruit de fond pour l'analyse des dommages des bâtiments de boumerdes suite au séisme du 21 mai 2003, Mémoires du Service Géologique de l'Algérie 12 (2004) 177–191.

[12] N. Stubbs, A general theory of non-destructive damage detection in structures, in: Structural Control, Springer, 1987, pp. 694–713.
[13] S. W. Doebling, C. R. Farrar, M. B. Prime, others, A summary review of vibration-based damage identification methods, Shock and vibration digest 30 (2) (1998) 91–105.
[14] O. Salawu, Detection of structural damage through changes in frequency: a review, Engineering structures 19 (9) (1997) 718–723.
[15] E. P. Carden, P. Fanning, Vibration based condition monitoring: a review, Structural Health Monitoring 3 (4) (2004) 355–377.
[16] K. Worden, J. Dulieu-Barton, An overview of intelligent fault detection in systems and structures, Structural Health Monitoring 3 (1) (2004) 85–98.
[17] B. Moaveni, X. He, J. P. Conte, J. I. Restrepo, Damage identification study of a seven-story full-scale building slice tested on the UCSD-NEES shake table, Structural Safety 32 (5) (2010) 347–356.
[18] B. Moaveni, A. Stavridis, G. Lombaert, J. P. Conte, P. B. Shing, Finite-element model updating for assessment of progressive damage in a 3-story infilled RC frame, Journal of Structural Engineering 139 (10) (2012) 1665–1674.
[19] D. Foti, V. Gattulli, F. Potenza, Output-Only Identification and Model Updating by Dynamic Testing in Unfavorable Conditions of a Seismically Damaged Building, Computer-Aided Civil and Infrastructure Engineering 29 (9) (2014) 659–675.
[20] N. Stubbs, S. Park, C. Sikorsky, S. Choi, A global non-destructive damage assessment methodology for civil engineering structures, International Journal of Systems Science 31 (11) (2000) 1361–1373.
[21] R. Rodriguez, J. A. Escobar, R. Gomez, Damage detection in instrumented structures without baseline modal parameters, Engineering Structures 32 (6) (2010) 1715–1722.
[22] A. Nozari, I. Behmanesh, S. Yousefianmoghadam, B. Moaveni, A. Stavridis, Effects of variability in ambient vibration data on model updating and damage identification of a 10-story building, Engineering Structures 151 (2017) 540–553.
[23] I. Behmanesh, B. Moaveni, C. Papadimitriou, Probabilistic damage identification of a designed 9-story building using modal data in the presence of modeling errors, Engineering Structures 131 (2017) 542–552.
[24] G. Hearn, R. B. Testa, Modal analysis for damage detection in structures, Journal of Structural Engineering 117 (10) (1991) 3042–3063.
[25] M. I. Friswell, Damage identification using inverse methods, Philosophical Transactions of the Royal Society of London A: Mathematical, Physical and Engineering Sciences 365 (1851) (2007) 393–410.
[26] J. Mottershead, M. Friswell, Model updating in structural dynamics: a survey, Journal of sound and vibration 167 (2) (1993) 347–375.
[27] I. Behmanesh, B. Moaveni, Probabilistic identification of simulated damage on the Dowling Hall footbridge through Bayesian finite element model updating, Structural Control and Health Monitoring 22 (3) (2015) 463–483.
[28] K. Worden, A. Lane, Damage identification using support vector machines, Smart Materials and Structures 10 (3) (2001) 540.
[29] D. Posenato, F. Lanata, D. Inaudi, I. F. C. Smith, Model-free data interpretation for continuous monitoring of complex structures, Advanced Engineering Informatics 22 (1) (2008) 135–144.
[30] I. Laory, T. N. Trinh, D. Posenato, I. F. C. Smith, Combined model-free data-interpretation methodologies for damage detection during continuous monitoring of structures, Journal of Computing in Civil Engineering 27 (6) (2013) 657–666.
[31] B. Xu, J. He, S. F. Masri, Data-Based Model-Free Hysteretic Restoring Force and Mass Identification for Dynamic Systems, Computer-Aided Civil and Infrastructure Engineering 30 (1) (2015) 2–18.
[32] J. W. van de Lindt, N. Nazari, Y. Li, Quantifying and accounting for aftershock hazard in performance-based earthquake engineering.
[33] A. Réveillère, P. Gehl, D. Seyedi, H. Modaressi, Development of seismic fragility curves for mainshock-damaged reinforced-concrete structures, 2012, p. 999.
[34] J.-S. Jeon, R. DesRoches, L. N. Lowes, I. Brilakis, Framework of aftershock fragility assessment–case studies: older california reinforced concrete building frames, Earthquake Engineering & Structural Dynamics 44 (15) (2015) 2617–2636.
[35] M. Raghunandan, A. B. Liel, N. Luco, Aftershock collapse vulnerability assessment of reinforced concrete frame structures, Earthquake Engineering & Structural Dynamics 44 (3) (2015) 419–439.
[36] K. Trevlopoulos, P. Guéguen, Period elongation-based framework for operative assessment of the variation of seismic vulnerability of reinforced concrete buildings during aftershock sequences, Soil Dynamics and Earthquake Engineering 84 (2016) 224–237.
[37] J.-A. Goulet, P. Kripakaran, I. F. C. Smith, Multimodel structural performance monitoring, Journal

of Structural Engineering 136 (10) (2010) 1309–1318.
[38] J.-A. Goulet, I. F. C. Smith, Structural identification with systematic errors and unknown uncertainty dependencies, Computers & Structures 128 (2013) 251–258.
[39] R. Pasquier, I. F. C. Smith, Robust system identification and model predictions in the presence of systematic uncertainty, Advanced Engineering Informatics 29 (4) (2015) 1096–1109.
[40] Y. Reuland, P. Lestuzzi, I. F. C. Smith, Data-interpretation methodologies for non-linear earthquake response predictions of damaged structures, Frontiers in Built Environment 3 (2017) 43.
[41] R. Pasquier, I. F. C. Smith, Iterative structural identification framework for evaluation of existing structures, Engineering Structures 106 (2016) 179–194.
[42] G. Grünthal, R. M. V. Musson, J. Schwarz, M. Stucchi, European Macroseismic Scale 1998, EMS-98. Cahiers du Centre Européen de Géodynamique et de Séismologie, Volume 19. (2001).
[43] S. Lagomarsino, S. Giovinazzi, Macroseismic and mechanical models for the vulnerability and damage assessment of current buildings, Bulletin of Earthquake Engineering 4 (4) (2006) 415–443.
[44] K. R. Popper, The logic of scientific discovery, Hutchinson, London, 1959.
[45] B. Raphael, I. F. C. Smith, Finding the right model for bridge diagnosis, in: Artificial intelligence in structural engineering, Springer, 1998, pp. 308–319.
[46] Y. Robert-Nicoud, B. Raphael, I. F. C. Smith, System identification through model composition and stochastic search, Journal of computing in civil engineering 19 (3) (2005) 239–247.
[47] I. F. C. Smith, Studies of Sensor-Data Interpretation for Asset Management of the Built Environment, Frontiers in Built Environment 2 (2016) 8.
[48] Z. Šidák, Rectangular confidence regions for the means of multivariate normal distributions, Journal of the American Statistical Association 62 (318) (1967) 626–633.
[49] S. G. S. Pai, A. Nussbaumer, I. F. C. Smith, Comparing structural identification methodologies for fatigue life prediction of a highway bridge, Frontiers in Built Environment 3 (2018) 73.
[50] A. Garofano, P. Lestuzzi, Seismic Assessment of a Historical Masonry Building in Switzerland: The Ancien Hôpital De Sion, International Journal of Architectural Heritage 10 (8) (2016) 975–992.
[51] K. Meguro, H. S. Tagel-Din, Applied element method used for large displacement structural analysis, Journal of Natural Disaster Science 24 (1) (2002) 25–34.
[52] H. Okamura, K. Maekawa, Nonlinear analysis and constitutive models of reinforced concrete, Gihodo, Tokyo 10.
[53] R. Guragain, A. Dixit, K. Meguro, Development of fragility functions for low strength masonry buildings in Nepal using applied element methods, in: 15th world conference of earthquake engineering, Lisbon, Portugal, 2012.
[54] K. Meguro, H. S. Tagel-Din, Applied element method used for large displacement structural analysis, Journal of Natural Disaster Science 24 (1) (2002) 25–34.
[55] A. Karbassi, M.-J. Nollet, Performance-Based Seismic Vulnerability Evaluation of Masonry Buildings Using Applied Element Method in a Nonlinear Dynamic-Based Analytical Procedure, Earthquake Spectra 29 (2) (2013) 399–426.
[56] A. Karbassi, P. Lestuzzi, Fragility analysis of existing unreinforced masonry buildings through a numerical-based methodology, The Open Civil Engineering Journal 6 (Suppl 1) (2012) M2.
[57] L. Diana, Y. Reuland, P. Lestuzzi, Seismic vulnerability assessment of sion cathedral(switzerland): an integrated approach to detect and evaluate local collapse mechanisms in heritage buildings, in: Prohitech" 17: 3rd international conference on protection of historical constructions, 2017.
[58] A. I. Zerin, A. Hosoda, H. Salem, K. M. Amanat, Seismic performance evaluation of masonry infilled reinforced concrete buildings utilizing verified masonry properties in applied element method, Journal of Advanced Concrete Technology 15 (6) (2017) 227–243.
[59] A. Elshaer, H. Mostafa, H. Salem, Progressive collapse assessment of multistory reinforced concrete structures subjected to seismic actions, KSCE Journal of Civil Engineering 21 (1) (2017) 184–194.
[60] C. Michel, A. Karbassi, P. Lestuzzi, Evaluation of the seismic retrofitting of an unreinforced masonry building using numerical modeling and ambient vibration measurements, Engineering Structures 158 (2018) 124–135.
[61] H. Tagel-Din, K. Meguro, Applied element method for dynamic large deformation analysis of structures, Doboku Gakkai Ronbunshu 2000 (661) (2000) 1–10.
[62] P. Fajfar, P. Gašperšič, The n2 method for the seismic damage analysis of rc buildings, Earthquake Engineering & Structural Dynamics 25 (1) (1996) 31–46.
[63] S. Antoniou, A. Rovithakis, R. Pinho, Development and verification of a fully adaptive pushover procedure, in: Proceedings of the Twelfth European Conference on Earthquake Engineering, 2002.
[64] S. Antoniou, R. Pinho, Advantages and limitations of adaptive and non-adaptive force-based pushover procedures, Journal of Earthquake Engineering 8 (04) (2004) 497–522.

[65] K. Beyer, M. Tondelli, S. Petry, S. Peloso, Dynamic testing of a four-storey building with reinforced concrete and unreinforced masonry walls: prediction, test results and data set, Bulletin of Earthquake Engineering 13 (10) (2015) 3015–3064.

[66] N. Ambraseys, P. Smit, J. Douglas, B. Margaris, R. Sigbjrnsson, S. Olafsson, P. Suhadolc, G. Costa, Internet site for European strong-motion data, Bollettino di Geofisica Teorica ed Applicata 45 (3) (2004) 113–129.

[67] C. Michel, B. Zapico, P. Lestuzzi, F. J. Molina, F. Weber, Quantification of fundamental frequency drop for unreinforced masonry buildings from dynamic tests, Earthquake Engineering & Structural Dynamics 40 (11) (2011) 1283–1296.

[68] A. Karbassi, P. Lestuzzi, Seismic risk for existing buildings in switzerland development of fragility curves for masonry buildings, Report prepared under contract to the Federal Office for the Environment. (FOEN) EPFL-REPORT-182359, Ecole Polytechnique Fdrale de Lausanne, Switzerland. (2012).

[69] M. Box, Simplified experimental design, Technometrics 13 (1) (1971) 19–31.

[70] L. Diana, A. Manno, P. Lestuzzi, S. Podestà, C. Luchini, Impact of displacement demand reliability for seismic vulnerability assessment at an urban scale, Soil Dynamics and Earthquake Engineering 112 (2018) 35–52.